Microphysical and Radiative Effects of Ice Clouds on Tropical Equilibrium States: A Two-Dimensional Cloud-Resolving Modeling Study

FAN PING

Laboratory of Cloud-Precipitation Physics and Severe Storms (LACS), Institute of Atmospheric Physics, Chinese Academy of Sciences, Beijing, China

ZHEXIAN LUO

Department of Geography, Nanjing University of Information Science and Technology, Nanjing, China

XIAOFAN LI

Joint Center for Satellite Data Assimilation, and NOAA/NESDIS/Center for Satellite Applications and Research, Camp Springs, Maryland

(Manuscript received 14 April 2006, in final form 9 October 2006)

ABSTRACT

The microphysical and radiative effects of ice clouds on tropical equilibrium states are investigated based on three two-dimensional cloud-resolving simulations imposed by zero vertical velocity and time-invariant zonal wind and sea surface temperature. An experiment without ice microphysics (ice microphysical and radiative effects; C00), another experiment without ice radiative effects (CI0), and the control experiment (CIR) are carried out. The model with cyclic lateral boundaries is integrated for 40 days to reach equilibrium states in all experiments. CI0 produces a colder and drier equilibrium state than CIR and C00 do through generating a larger IR cooling, a larger vapor condensation rate, and consuming a larger amount of water vapor. A larger surface rain rate occurs in CI0 than in CIR and C00. The ice radiative effects on thermodynamic equilibrium states are stronger than the ice microphysical effects so that the exclusion of ice microphysics yields a colder and drier equilibrium state in C00 than in CIR. The ice radiative effects and the ice microphysical effects on surface rainfall processes are largely offset, which leads to similar zonal-mean surface rain rates in C00 and CIR.

1. Introduction

The interaction between convection and environmental dynamics affects tropical climate through thermodynamic, radiative, and cloud microphysical processes. The studies of climate equilibrium states with equilibrium cloud-resolving model simulations enhance the understanding of associated controlling physical processes. Tropical climate could be a cold and dry equilibrium state (e.g., Sui et al. 1994) or a warm and humid equilibrium state (e.g., Grabowski et al. 1996), largely depending on surface processes (e.g., Xu and Randall 1999; Tao et al. 1999), sea surface temperature (e.g., Wu and Moncrieff 1999; Gao et al. 2007), vertical wind shear (e.g., Shie et al. 2003), and radiative processes (e.g., Robe and Emanuel 1996; Gao et al. 2007).

Ice clouds have important impacts on tropical climate by changing atmospheric moisture and heat through ice microphysical processes and associated heat release as well as through radiative processes. The cloud-resolving simulations of squall lines (e.g., Yoshizaki 1986; Nicholls 1987; Fovell and Ogura 1988; Tao and Simpson 1989; McCumber et al. 1991; Tao et al. 1991; Liu et al. 1997; Grabowski et al. 1999; Wu et al. 1999; Li

Corresponding author address: Dr. F. Ping, Laboratory of Cloud-Precipitation Physics and Severe Storms (LACS), Institute of Atmospheric Physics, Chinese Academy of Sciences, Beijing 100029, China.
E-mail: pingf@mail.iap.ac.cn

DOI: 10.1175/MWR3419.1

et al. 1999; Grabowski and Moncrieff 2001; Grabowski 2003) have demonstrated the importance of ice microphysics in the development of tropical convection. Grabowski (2000) showed that the cloud microphysics has a minor effect on the equilibrium states of atmosphere in the cloud-resolving simulations with time-invariant sea surface temperature gradient and prescribed radiative cooling. On the other hand, Wu (2002) found that the coupled cloud–ocean model simulation with a larger ice fall speed produces a colder and drier equilibrium state than the simulation with a smaller ice fall speed does.

Recently, Gao et al. (2006) examined the effects of ice microphysics on the tropical atmosphere using the two-dimensional cloud-resolving model (the same model used in this study) and found that the experiment without ice microphysics produces a colder and more humid atmosphere, a larger amount of cloud water, and a lower surface rain rate than does the experiment with ice microphysics. However, the main limitation of Gao et al.'s (2006) study is that the zonally uniform vertical velocity calculated by using the observation data from Tropical Ocean Global Atmosphere Coupled Ocean–Atmosphere Response Experiment (TOGA COARE) includes the ice effects, while it is imposed in both simulations that include and exclude ice microphysics. In this study, a zero zonal-mean vertical velocity is imposed in both simulations with and without ice microphysics to explore the ice effects on tropical thermodynamic, cloud, and surface rainfall processes, and the results are also compared with Gao et al. (2006) to examine the sensitivity of the ice effects to imposed vertical velocity.

Gao et al. (2006) did not distinguish the microphysical and radiative effects of ice clouds because they simply excluded ice microphysics from their simulation. The ice microphysical effects here include thermal effects associated with the latent heat release and moist effects associated with the exchange between vapor and cloud hydrometeors. In this study, the simulation without ice microphysics (ice microphysical and radiative effects), the simulation without ice radiative effects, and the control simulation are conducted and compared to analyze the ice microphysical and radiative effects on tropical equilibrium states. In the next section, the model and experiments will be briefly described. The results are presented in section 3. A summary is given in section 4.

2. Model and experiment design

The cloud-resolving model used in this study was originally developed by Soong and Ogura (1980), Soong and Tao (1980), and Tao and Simpson (1993). The two-dimensional version of the model used by Sui et al. (1994, 1998) and further modified by Li et al. (1999) is used in this study. The governing equations and model setup can be found in Li et al. (1999, 2002a). The model includes prognostic equations for perturbation zonal wind and vertical velocity, potential temperature, specific humidity, and mixing ratios of cloud water (q_c), raindrops (q_r), cloud ice (q_i), snow (q_s), and graupel (q_g). The cloud microphysical processes in the model are determined by the microphysical parameterization schemes from Rutledge and Hobbs (1983, 1984), Lin et al. (1983), Tao et al. (1989), and Krueger et al. (1995). The major water microphysical processes are vapor condensation (P_{CND}), collection of cloud water by rain (P_{RACW}), autoconversion of cloud water to rain (P_{RAUT}), and evaporation of rain (P_{REVP}), whereas the major ice microphysical processes are vapor deposition to ice (P_{DEP}), snow (P_{SDEP}), and graupel (P_{GDEP}), depositional growth of snow from cloud ice (P_{SFI}), conversion of cloud ice to snow (P_{SAUT}), and accretion of snow by graupel (P_{GACS}). The exchanges between water and ice hydrometeors are described by accretion of cloud water by snow (P_{SACW}) and graupel (P_{GACW}), and melting of snow (P_{SMLT}) and graupel (P_{GMLT}) to rain.

The model also includes interactive solar (Chou et al. 1998) and thermal infrared (Chou et al. 1991; Chou and Suarez 1994) radiation parameterization schemes that are performed every 3 min. The water and ice clouds affect radiation budgets through parameterized cloud optical properties in parameterized solar and infrared radiation calculations (Sui et al. 1998), where the parameterized cloud optical thickness is a function of cloud content.

The cloud-resolving model cannot simulate large-scale circulations because of the small horizontal domain. Thus, the observed large-scale variables such as vertical velocity and zonal wind are imposed in the model to examine the responses of the model to the imposed large-scale forcing (Soong and Ogura 1980; also see the detailed discussion in Li et al. 1999). As a special case, the model is forced by a zonally uniform zero vertical velocity, a time-invariant zonal wind of 4 m s^{-1}, and a constant sea surface temperature of 29°C in this study. The model uses cyclic lateral boundaries. The vertical velocity, vertical gradients of potential temperature, specific humidity, and mixing ratios of cloud hydrometeors in the model are set to zero at both the upper and lower boundaries (Soong and Ogura 1980). The surface momentum, heat, and evaporation fluxes are calculated from bulk formulations using predicted wind, temperature, and specific humidity (Soong

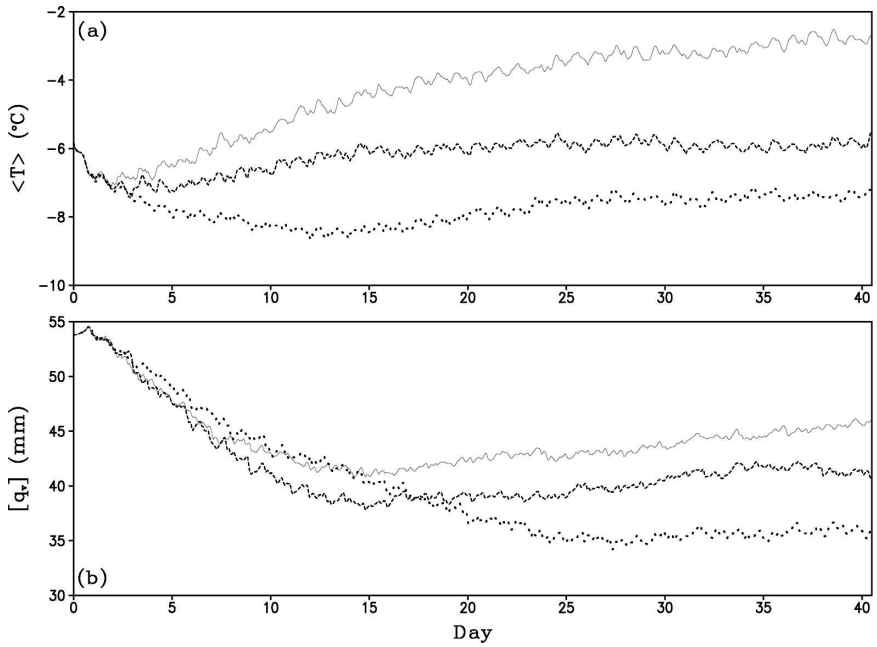

FIG. 1. Time series of (a) mass-weighted mean temperature (°C) and (b) precipitable water (mm) in CIR (solid), C00 (dashed), and CI0 (dotted).

and Ogura 1980). The vertical profiles of temperature and specific humidity observed at 1.75°S, 156°E during TOGA COARE at 0400 LST 19 December 1992 (Sui et al. 1997) are used as the initial conditions. The initial mass-weighted temperature and precipitable water are −5.8°C and 53.8 mm, respectively. The initial convective available potential energy for a reversible moist process calculated using the formation from Li et al. (2002b) is 107.5 J kg^{-1}. The horizontal domain is 768 km with a horizontal grid resolution of 1.5 km. The top model level is 42 mb. The vertical grid resolution ranges from about 200 m near the surface to about 1 km near 100 mb. The time step is 12 s.

Three experiments are carried out. The control experiment (CIR) includes ice microphysics. Experiment CI0 is identical to CIR except that CI0 excludes the radiative effects of ice clouds by setting mixing ratios of ice hydrometeors to zero in the calculation of radiation. The comparison between CI0 and CIR shows the radiative effects of ice clouds on tropical equilibrium states. Experiment C00 excludes ice cloud variables and associated ice microphysical and radiative processes by turning off the ice microphysics scheme during the model integration. The comparison between C00 and CI0 shows the microphysical effects of ice clouds on the tropical equilibrium states. The comparison between C00 and CIR reveals both microphysical and radiative effects of ice clouds on tropical equilibrium states, which are used to evaluate the results in Gao et al. (2006), where TOGA COARE–derived vertical velocity is imposed during the model integrations. The model is integrated for 40.5 days to reach a quasi-equilibrium state.

3. Results

a. Thermodynamic equilibrium states

The time series of zonal and mass-weighted mean temperatures and precipitable water (PW) is shown in Fig. 1. Mean temperature and PW reach quasi-equilibrium states in the 3 experiments during the 40-day integrations. Zonal and mass-weighted mean temperatures averaged from 31 to 40 days are −3.0°C in CIR, −7.4°C in CI0, and −5.9°C in C00. Zonal-mean precipitable waters averaged from day 31 to day 40 are 44.9 mm in CIR, 35.7 mm in CI0, and 41.4 mm in C00. The negative temperature difference between C00 and CIR (i.e., C00 − CIR) reveals that the exclusion of ice microphysics produces a cold equilibrium state, which is consistent with the result found by Gao et al. (2006). The negative PW difference for C00 − CIR shows that the exclusion of ice microphysical and radiative effects generates a dry equilibrium state, which is different from the moist state found in Gao et al. (2006). Gao et al. (2006) analyzed the mass-weighted mean heat and PW budgets and found that the simulation excluding ice microphysics produces a colder and more humid state than the simulation including ice microphysics does

TABLE 1. Differences in (a) zonal-mean mass-weighted mean temperature budget (°C day^{-1}) and (b) PW budget (mm day^{-1}) for C00 − CIR, CI0 − CIR, and C00 − CI0 averaged from the first 30-day simulation data.

	C00 − CIR	CI0 − CIR	C00 − CI0
(a) Zonal-mean mass-weighted mean temperature budget			
Temperature tendency	−0.091	−0.146	0.055
Condensational heating	0.032	0.223	−0.191
Radiative heating	−0.113	−0.382	0.269
Surface sensible heat flux	−0.009	0.013	−0.022
(b) PW budget			
PW tendency	−0.098	−0.212	0.114
Condensation	−0.283	−0.709	0.426
Surface evaporation flux	0.186	0.437	−0.251

simply because the exclusion of ice hydrometeors causes a smaller cloud heating and consumes a smaller amount of water vapor. To understand the physical processes that are responsible for temperature and PW differences in this study, zonal-mean heat and moisture budgets are analyzed next.

Following Li et al. (1999), zonal-mean heat and vapor budgets can be expressed by

$$\frac{\partial\langle\overline{T}\rangle}{\partial t} = \frac{\langle\overline{Q}_{\rm cn}\rangle}{c_p} + \frac{\langle\overline{Q}_R\rangle}{c_p} + \overline{H}_s \quad \text{and} \tag{1a}$$

$$\frac{\partial[\overline{q}_v]}{\partial t} = -[\overline{S}_{\rm qv}] + \overline{E}_s. \tag{1b}$$

Here, $\langle(\,)\rangle = [(\,)]/[1]$, where $[(\,)] = \int_0^{z_t} (\,)\overline{\rho}\, dz$ and z_t is the model top, is a mass integration; T and q_v are air temperature and specific humidity, respectively; $[\overline{q}_v]$ is PW; c_p is the specific heat of dry air at constant pressure p; $\overline{\rho}$ is a mean air density, which is a function of height only; $Q_{\rm cn}$ denotes the net latent heat release; Q_R is the radiative heating rate due to the convergence of net flux of solar and infrared radiative fluxes; H_s is surface sensible heat flux; $S_{\rm qv}$ is the sum of vapor condensation, deposition to cloud ice, snow, and graupel, and evaporation of rain and melting precipitation ice; E_s is surface evaporation flux; and the overbar indicates the zonal mean over the cyclic model domain. The temperature tendency is determined by condensational heating, radiative heating, and surface sensible heat flux, whereas the PW tendency is determined by condensation and surface evaporation flux. The data in the first 30 days are used to calculate the heat and moisture budgets.

The negative radiation difference is responsible for the negative temperature tendency difference for CI0 − CIR whereas the negative condensation difference accounts for the negative PW tendency difference (Table 1). This indicates that the simulation that excludes the ice radiative effects yields a larger IR cooling rate through allowing more outgoing IR radiation from the atmosphere than the simulation that includes the ice radiative effects does. The negative radiation difference for CI0 − CIR is mainly determined by the negative difference in zonal-mean infrared cooling, which is in turn controlled by the negative IR difference in clear-sky regions (Table 2). The negative difference in clear-sky IR cooling for CI0 − CIR may be because the clear sky covers much larger areas in CI0 than in CIR (Table 3).

The positive radiation difference is responsible for the positive temperature tendency difference for C00 − CI0 whereas the positive condensation difference accounts for the positive PW tendency difference (Table 1). The positive difference in IR cooling in cloudy regions explains the positive temperature tendency difference (Table 2). The positive difference in cloudy IR

TABLE 2. Temperature tendency differences (°C day^{-1}) caused by solar heating and IR cooling from zonal means, clear-sky regions, and cloudy regions for C00 − CIR, CI0 − CIR, and C00 − CI0 averaged from the first 30-day simulation data.

	C00 − CIR	CI0 − CIR	C00 − CI0
Zonal-mean solar heating	−0.011	0.002	−0.013
Zonal-mean IR cooling	−0.103	−0.384	0.281
Solar heating in clear-sky regions	0.169	0.101	0.068
IR cooling in clear-sky regions	−0.345	−0.300	−0.045
Solar heating in cloudy regions	−0.180	−0.099	−0.081
IR cooling in cloudy regions	0.243	−0.084	0.327

TABLE 3. Fractional cloud coverage (%), IWP, LWP (mm), P_s, Q_{WVT}, Q_{WVF}, Q_{WVE}, and Q_{CM} (mm h^{-1}) over clear-sky regions, raining stratiform regions, convective regions, and nonraining stratiform regions averaged from days 31 to 40 in (a) CIR, (b) CI0, and (c) C00.

(a)	Clear-sky regions	Raining stratiform regions	Convective regions	Nonraining stratiform regions	Zonal mean
			(a) CIR		
Fractional coverage	40.7	5.8	4.2	50.1	100
IWP	0.000	0.018	0.005	0.036	0.06
LWP	0.000	0.041	0.040	0.005	0.086
P_s	0.000	0.056	0.074	0.000	0.130
Q_{WVT}	0.013	0.019	−0.011	−0.021	0.000
Q_{WVF}	−0.088	0.007	0.116	−0.034	0.000
Q_{WVE}	0.074	0.004	0.002	0.053	0.134
Q_{CM}	0.000	0.025	−0.033	0.002	−0.005
			(b) CI0		
Fractional coverage	64.3	4.5	3.2	28.0	100
IWP	0.000	0.028	0.011	0.029	0.069
LWP	0.000	0.032	0.048	0.005	0.085
P_s	0.000	0.065	0.121	0.000	0.186
Q_{WVT}	0.001	0.030	−0.024	0.003	0.010
Q_{WVF}	−0.125	−0.018	0.197	−0.053	0.000
Q_{WVE}	0.122	0.007	0.005	0.044	0.178
Q_{CM}	0.002	0.046	−0.056	0.006	−0.003
			(c) C00		
Fractional coverage	72.6	2.3	3.4	21.5	100
IWP	0.000	0.000	0.000	0.000	0.000
LWP	0.000	0.039	0.052	0.026	0.117
P_s	0.000	0.038	0.086	0.000	0.124
Q_{WVT}	0.007	0.009	−0.008	−0.006	0.002
Q_{WVF}	0.126	0.018	0.111	−0.005	0.000
Q_{WVE}	0.117	0.003	0.003	0.024	0.147
Q_{CM}	0.002	0.008	−0.021	−0.012	−0.023

cooling for C00 − CI0 may be because the clouds cover smaller areas in C00 (sum of fractional coverage of raining stratiform regions, convective regions, and nonraining stratiform regions is 27.4%) than in CI0 (35.7%) (Table 3). Note that the ice microphysical effects on thermodynamic equilibrium states are taken by the radiative change associated with water hydrometeors since the radiative effects associated with ice clouds are excluded in both experiments C00 and CI0.

Tables 1 and 2 show that the differences in heat and moisture budgets for C00 − CIR are similar to those for CI0 − CIR although the former magnitudes are smaller than the latter magnitudes. This indicates that the radiative effects of ice clouds on thermodynamic equilibrium states are dominant and the microphysical effects of ice clouds are secondary.

It should be noticed that the different tropical equilibrium states between CI0 and CIR are mainly contributed to by the different zonally averaged radiative heating profiles. Thus, the zonally averaged radiative heating profile constructed from CIR should be included in CI0 to examine the role of ice cloud–radiation interaction on tropical equilibrium states. However, there are two technical issues with the experiment of ice cloud–radiation interaction. First, because the ice clouds (above 650 mb) and water clouds (below 250 mb) coexist in the midatmosphere, it is difficult to construct the ice radiative heating profile from the control experiment. Second, the experiment with the prescribed ice radiative heating profile allows the water cloud–radiation interaction, which leads to an incorrect radiation calculation in the layers where ice and water clouds coexist.

b. Surface rainfall and cloud processes

To analyze the ice microphysical and radiative effects on surface rainfall processes, the zonal-mean surface rainfall equation is analyzed using the equilibrium data from days 31 to 40 for the 3 experiments. Following a similar derivation in Gao et al. (2005), surface rain rate (P_s) can be expressed as

$$P_s = Q_{WVT} + Q_{WVF} + Q_{WVE} + Q_{CM}, \qquad (2)$$

where Q_{WVT} $(=-\partial[q_v]/\partial t)$ is the local vapor change; Q_{WVF}

$$\left\{=-\left(\overline{u}^{o}\frac{\partial\overline{q_v}}{\partial x}\right)-\left[\frac{\partial(uq_v')}{\partial x}\right]-\left(\overline{u}^{o}\frac{\partial q'}{\partial x}\right)-\left(w'\frac{\partial\overline{q_v}}{\partial z}\right)\right\}$$

is vapor convergence; Q_{WVE} is the surface evaporation rate; Q_{CM}

$$\left[=-\frac{\partial[q_5]}{\partial t}-\left(u\frac{\partial q_5}{\partial x}\right)-\left(w\frac{\partial q_5}{\partial z}\right)\right]$$

is the sum of local hydrometeor change and hydrometeor convergence; u and w are zonal and vertical air wind components, respectively; $q_5 = q_c + q_r + q_i + q_s + q_g$, where q_c, q_r, q_i, q_s, and q_g are the mixing ratios of cloud water (small cloud droplets), raindrops, cloud ice (small ice crystals), snow (density 0.1 g cm^{-3}), and graupel (density 0.4 g cm^{-3}), respectively; a prime denotes a perturbation from the zonal mean; and the superscript o indicates an imposed forcing.

Table 3 shows the fractional cloud coverage, ice water path (IWP), liquid water path (LWP), P_s, Q_{WVT}, Q_{WVF}, Q_{WVE}, and Q_{CM} over clear-sky regions, raining stratiform regions, convective regions, and nonraining stratiform regions averaged from days 31 to 40 in the 3 experiments. Note that the partitioning method proposed by Sui et al. (1994) is applied to each grid point to determine the area type (clear sky, raining stratiform, convective, or nonraining stratiform) and the summations of grid points, and other quantities (e.g., IWP, LWP, and the others) are taken and divided by the total zonal grid points (512) and the length of the hourly data (240) so that the sums of the values in columns 2–5 in Table 3 are the zonal mean in column 6.

The exclusion of ice radiative effects increases IWP in raining stratiform and convective regions and thus zonal-mean IWP (Tables 3a, b) because the exclusion of ice radiative effects produces a larger deposition rate ($P_{\mathrm{DEP}} + P_{\mathrm{SDEP}} + P_{\mathrm{GDEP}} = 0.053$ mm h^{-1}) than the inclusion of ice radiative effects does ($P_{\mathrm{DEP}} + P_{\mathrm{SDEP}} + P_{\mathrm{GDEP}} = 0.042$ mm h^{-1}) (Figs. 2a,b). The exclusion of ice microphysical effects mainly enhances LWP in nonraining stratiform regions and thus zonal-mean LWP (Tables 3b, c). The exclusion of ice microphysical and radiative effects enhances LWP in nonraining stratiform and convective regions and thus zonal-mean LWP (Tables 3a, c). The analysis of the cloud microphysics budget (Fig. 2c) reveals that the larger zonal-mean LWP in C00 comes from the larger amount of cloud water that is accounted for by the cloud water source S_{qc} (0.024 mm h^{-1}), where S_{qc} is the sum of microphysical processes in the cloud water budget (Li et al. 1999). This is consistent with the result found in Gao et al. (2006).

The exclusion of ice radiative effects leads to a larger zonal-mean surface rain rate in CI0 than in CIR (Tables 3a, b). CI0 produces a larger convective rain rate than CIR does because CI0 has a larger vapor convergence than CIR does. Because of the cyclic lateral boundary conditions, the larger vapor convergence in convective regions is caused by the larger vapor divergence in clear-sky regions in CI0 that is balanced by the larger surface evaporation in CI0, compared with that of CIR. The larger surface evaporation in clear-sky regions is caused by drier air and larger clear-sky coverage in CI0 since sea surface temperature is fixed during the integration. The analysis of cloud microphysics budgets (Figs. 2a,b) shows that the exclusion of ice radiative effects produces colder temperatures that lead to larger vapor condensation rates and thus larger surface rain rates than the inclusion of ice radiative effects does.

The exclusion of ice microphysical effects yields a smaller zonal-mean surface rain rate in C00 than in CI0 (Tables 3b, c). C00 produces both smaller convective and stratiform rain rates than CI0 does because it has a smaller vapor convergence in convective regions and smaller positive values of Q_{WVT} and Q_{CM} in raining stratiform regions. In clear-sky regions, vapor divergences in the two experiments are similar. In nonraining stratiform regions, the vapor divergence in C00 is one order of magnitude smaller than that in CI0 because the surface evaporation rate is smaller in C00. Compared with CI0, the smaller surface evaporation rate in C00 is caused by more humid air and smaller coverage of nonraining stratiform regions. The analysis of cloud microphysics budgets (Figs. 2b,c) reveals that the exclusion of ice microphysical effects generates a smaller vapor condensation rate (P_{CND}) in C00 than in CI0 because C00 produces warmer atmosphere than CI0 does (Fig. 1a). Thus, the smaller vapor condensation rate leads to the smaller surface rain rate in C00 than in CI0.

The exclusion of ice microphysical and radiative effects in simulation produces a slightly smaller zonal-mean surface rain rate in C00 than in CIR (Tables 3a, c), indicating that the ice microphysical effects and ice radiative effects on surface rainfall processes are cancelled out. The difference (~5%) here is less significant than the difference (~20%) shown in Gao et al. (2007). The equilibrium zonal-mean surface rain rate is less sensitive to ice microphysics in the simulation imposed by zero vertical velocity than in the simulation imposed by nonzero vertical velocity. The cloud microphysical budget in the simulation with ice microphysics and imposed nonzero vertical velocity (Gao et al. 2006, Fig.

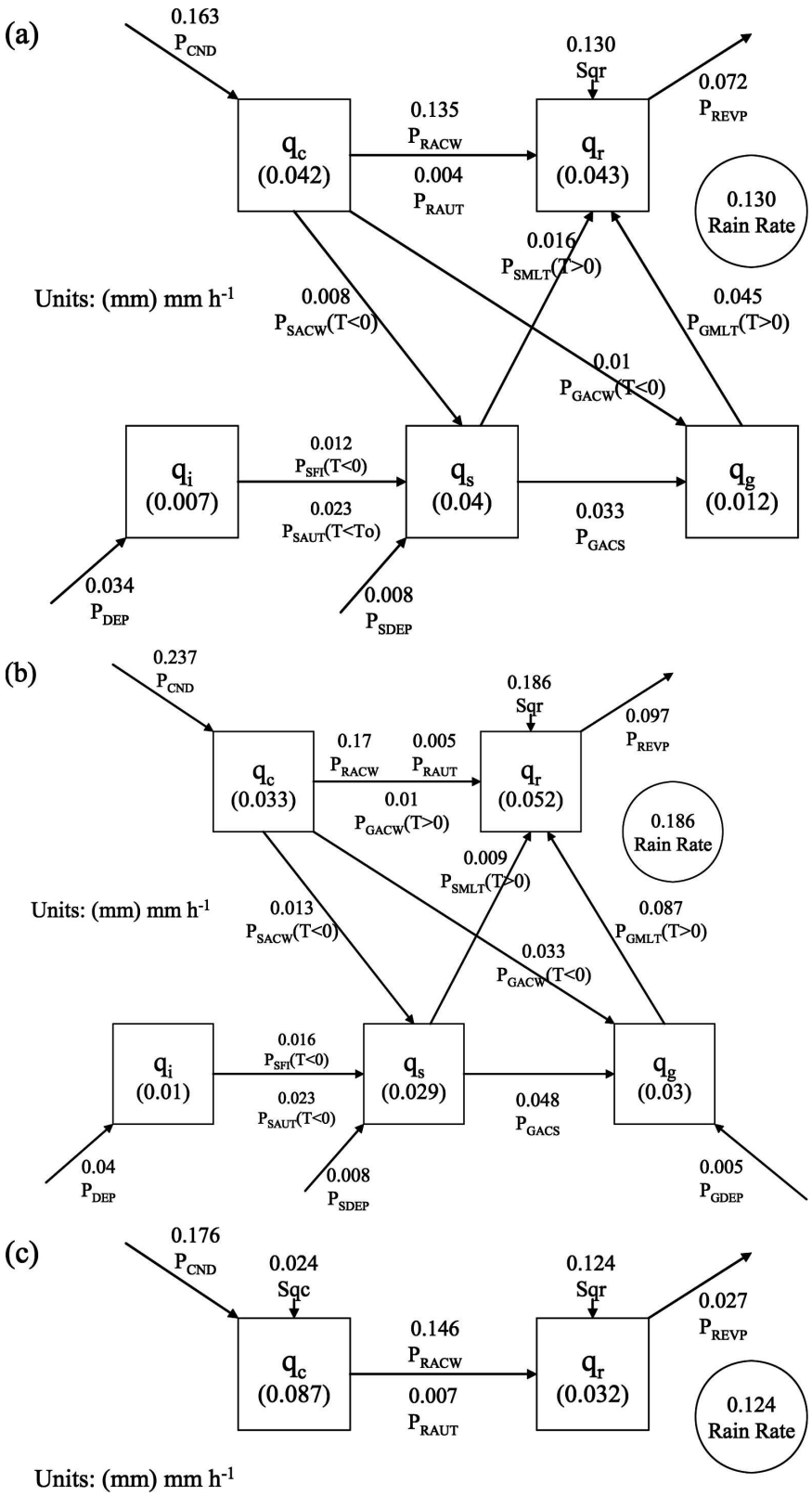

FIG. 2. Cloud microphysics budgets averaged from days 35 to 40 in (a) CIR, (b) CI0, and (c) C00. Here T is air temperature (°C); S_{qc} and S_{qr} are sums of microphysical rates in cloud water and raindrop budgets, respectively. Units for cloud hydrometeors and conversions are mm and mm h^{-1}, respectively.

3a) shows that the melting of precipitation ice ($P_{SMLT} + P_{GMLT} = 0.23$ mm h^{-1}) accounts for about 40% of the total rain source ($P_{RACW} + P_{RAUT} + P_{SMLT} + P_{GMLT} = 0.58$ mm h^{-1}). The cloud microphysical budget in the simulation with ice microphysics and imposed zero vertical velocity (Fig. 2a) reveals that the melting of precipitation ice ($P_{SMLT} + P_{GMLT} = 0.061$ mm h^{-1}) accounts for about 3% of the total rain source ($P_{RACW} + P_{RAUT} + P_{SMLT} + P_{GMLT} = 0.200$ mm h^{-1}). This indicates that ice microphysics plays a minor role in producing rainfall when the model is imposed by zero vertical velocity.

4. Summary

The microphysical and radiative effects of ice clouds on tropical equilibrium states are analyzed based on a series of two-dimensional cloud-resolving simulations that are imposed by zero vertical velocity and constant zonal wind and sea surface temperature. Experiment CI0 excludes radiative effects associated with ice clouds whereas experiment C00 excludes ice cloud variables and associated microphysical and radiative effects. These experiments are compared with CIR in this study. The model is integrated for 40 days to reach quasi-equilibrium states in all experiments.

The exclusion of ice radiative effects produces a colder and drier equilibrium state in CI0 than in CIR through more IR cooling and more consumption of water vapor in CI0. The exclusion of ice microphysical effects generates a warmer and more humid equilibrium state in C00 than in CI0 through less IR cooling associated with water clouds and less consumption of water vapor in C00. The ice radiative effects on thermodynamic equilibrium states are stronger than the ice microphysical effects. Thus, the exclusion of ice microphysics yields the colder and drier equilibrium state in C00 than in CIR.

The exclusion of ice radiative effects produces the colder temperature, larger vapor condensation rate, and thus larger zonal-mean rain rate in CI0 than in CIR, whereas the exclusion of ice microphysical effects generates the warm temperature, smaller vapor condensation rate, and thus smaller surface rain rate in C00 than in CI0. The ice radiative effects and the ice microphysical effects on surface rainfall processes are largely cancelled out. Thus, the exclusion of ice microphysical and radiative effects yields a slightly smaller zonal-mean surface rain rate in C00 than in CIR.

The effects of ice microphysics on tropical equilibrium states are analyzed in the simulations imposed by zero vertical velocity in this study in comparison with those in the simulations imposed by TOGA COARE–derived vertical velocity in Gao et al. (2006). The results here and in Gao et al. (2006) show similarities. The similarities include the fact that the exclusion of ice microphysics yields a cold temperature bias and enhances the cloud water amount. The difference between this study and Gao et al. (2006) is that the exclusion of ice microphysics in the simulation with the zero vertical velocity in this study produces a dry bias whereas the exclusion of ice microphysics in the simulation with the nonzero vertical velocity in Gao et al. (2006) generates a weak moist bias.

It should be noted that the microphysical and radiative effects of ice clouds on tropical equilibrium states are investigated with a set of cloud microphysics parameterization schemes (Rutledge and Hobbs 1983, 1984; Lin et al. 1983; Tao et al. 1989; Krueger et al. 1995). Li et al. (1999) showed that different ice microphysics parameterization schemes may produce different amounts of ice hydrometeors that may lead to different latent heat and radiative effects. Thus, different sets of cloud microphysics parameterization schemes may be used to study the microphysical and radiative effects of ice clouds on tropical equilibrium states.

Acknowledgments. The authors thank Dr. W.-K. Tao at NASA GSFC for his cloud-resolving model and two reviewers for their constructive comments. F. Ping and Z. Luo are supported by the National Natural Sciences Foundation of China under the Grants 40333028 and 40305010 and the National Key Basic Research and Development Project of China Grant 2004CB418301.

REFERENCES

Chou, M.-D., and M. J. Suarez, 1994: An efficient thermal infrared radiation parameterization for use in general circulation models. NASA Tech. Memo. 104606, Vol. 3, 85 pp. [Available from NASA Goddard Space Flight Center, Code 913, Greenbelt, MD 20771.]

——, D. P. Kratz, and W. Ridgway, 1991: Infrared radiation parameterizations in numerical climate models. *J. Climate,* **4,** 424–437.

——, M. J. Suarez, C.-H. Ho, M. M.-H. Yan, and K.-T. Lee, 1998: Parameterizations for cloud overlapping and shortwave single-scattering properties for use in general circulation and cloud ensemble models. *J. Climate,* **11,** 202–214.

Fovell, R. G., and Y. Ogura, 1988: Numerical simulation of a midlatitude squall line in two dimensions. *J. Atmos. Sci.,* **45,** 3846–3879.

Gao, S., X. Cui, Y. Zhou, and X. Li, 2005: Surface rainfall processes as simulated in a cloud-resolving model. *J. Geophys. Res.,* **110,** D10202, doi:10.1029/2004JD005467.

——, L. Ran, and X. Li, 2006: Impacts of ice microphysics on rainfall and thermodynamic processes in the tropical deep convective regime: A 2D cloud-resolving modeling study. *Mon. Wea. Rev.,* **134,** 3015–3024.

——, Y. Zhou, and X. Li, 2007: Effects of diurnal variations on

tropical equilibrium states: A two-dimensional cloud-resolving modeling study. *J. Atmos. Sci.,* **64,** 656–664.

Grabowski, W. W., 2000: Cloud microphysics and the tropical climate: Cloud-resolving model perspective. *J. Climate,* **13,** 2306–2322.

——, 2003: Impact of ice microphysics on multiscale organization of tropical convection in two-dimensional cloud-resolving simulations. *Quart. J. Roy. Meteor. Soc.,* **129,** 67–81.

——, and M. W. Moncrieff, 2001: Large-scale organization of tropical convection in two-dimensional explicit numerical simulations. *Quart. J. Roy. Meteor. Soc.,* **127,** 445–468.

——, ——, and J. T. Kiehl, 1996: Long-term behaviour of precipitating tropical cloud systems: A numerical study. *Quart. J. Roy. Meteor. Soc.,* **122,** 1019–1042.

——, X. Wu, and M. W. Moncrieff, 1999: Cloud resolving modeling of tropical cloud systems during Phase III of GATE. Part III: Effects of cloud microphysics. *J. Atmos. Sci.,* **56,** 2384–2402.

Krueger, S. K., Q. Fu, K. N. Liou, and H.-N. S. Chin, 1995: Improvements of an ice-phase microphysics parameterization for use in numerical simulations of tropical convection. *J. Appl. Meteor.,* **34,** 281–287.

Li, X., C.-H. Sui, K.-M. Lau, and M.-D. Chou, 1999: Large-scale forcing and cloud–radiation interaction in the tropical deep convective regime. *J. Atmos. Sci.,* **56,** 3028–3042.

——, ——, and ——, 2002a: Dominant cloud microphysical processes in a tropical oceanic convective system: A 2D cloud resolving modeling study. *Mon. Wea. Rev.,* **130,** 2481–2491.

——, ——, and ——, 2002b: Interactions between tropical convection and its environment: An energetics analysis of a 2D cloud resolving simulation. *J. Atmos. Sci.,* **59,** 1712–1722.

Lin, Y.-L., R. D. Farley, and H. D. Orville, 1983: Bulk parameterization of the snow field in a cloud model. *J. Climate Appl. Meteor.,* **22,** 1065–1092.

Liu, C., M. W. Moncrieff, and E. J. Zipser, 1997: Dynamic influence of microphysics in tropical squall lines: A numerical study. *Mon. Wea. Rev.,* **125,** 2193–2210.

McCumber, M., W.-K. Tao, J. Simpson, R. Penc, and S.-T. Soong, 1991: Comparison of ice-phase microphysical parameterization schemes using numerical simulations of tropical convection. *J. Appl. Meteor.,* **30,** 985–1004.

Nicholls, M. E., 1987: A comparison of the results of a two-dimensional numerical simulation of a tropical squall line with observations. *Mon. Wea. Rev.,* **115,** 3055–3077.

Robe, F. R., and K. A. Emanuel, 1996: Moist convective scaling: Some inferences from three-dimensional cloud ensemble simulations. *J. Atmos. Sci.,* **53,** 3265–3275.

Rutledge, S. A., and P. V. Hobbs, 1983: The mesoscale and microscale structure and organization of clouds and precipitation in midlatitude cyclones. VIII: A model for the "seeder-feeder" process in warm-frontal rainbands. *J. Atmos. Sci.,* **40,** 1185–1206.

——, and ——, 1984: The mesoscale and microscale structure and organization of clouds and precipitation in midlatitude cyclones. XII: A diagnostic modeling study of precipitation development in narrow cold-frontal rainbands. *J. Atmos. Sci.,* **41,** 2949–2972.

Shie, C.-L., W.-K. Tao, J. Simpson, and C.-H. Sui, 2003: Quasi-equilibrium states in the Tropics simulated by a cloud-resolving model. Part I: Specific features and budget analysis. *J. Climate,* **16,** 817–833.

Soong, S.-T., and Y. Ogura, 1980: Response of tradewind cumuli to large-scale processes. *J. Atmos. Sci.,* **37,** 2035–2050.

——, and W.-K. Tao, 1980: Response of deep tropical cumulus clouds to mesoscale processes. *J. Atmos. Sci.,* **37,** 2016–2034.

Sui, C.-H., K.-M. Lau, W.-K. Tao, and J. Simpson, 1994: The tropical water and energy cycles in a cumulus ensemble model. Part I: Equilibrium climate. *J. Atmos. Sci.,* **51,** 711–728.

——, ——, Y. N. Takayabu, and D. A. Short, 1997: Diurnal variations in tropical oceanic cumulus ensemble during TOGA COARE. *J. Atmos. Sci.,* **54,** 639–655.

——, X. Li, and K.-M. Lau, 1998: Radiative–convective processes in simulated diurnal variations of tropical oceanic convection. *J. Atmos. Sci.,* **55,** 2345–2357.

Tao, W.-K., and J. Simpson, 1989: Modeling study of a tropical squall-type convective line. *J. Atmos. Sci.,* **46,** 177–202.

——, and ——, 1993: The Goddard Cumulus Ensemble model. Part I: Model description. *Terr. Atmos. Oceanic Sci.,* **4,** 35–72.

——, ——, and M. McCumber, 1989: An ice-water saturation adjustment. *Mon. Wea. Rev.,* **117,** 231–235.

——, ——, and S.-T. Soong, 1991: Numerical simulation of a subtropical squall line over the Taiwan Strait. *Mon. Wea. Rev.,* **119,** 2699–2723.

——, ——, C.-H. Sui, C.-L. Shie, B. Zhou, K.-M. Lau, and M. Moncrieff, 1999: Equilibrium states simulated by cloud-resolving models. *J. Atmos. Sci.,* **56,** 3128–3139.

Wu, X., 2002: Effects of ice microphysics on tropical radiative–convective–oceanic quasi-equilibrium states. *J. Atmos. Sci.,* **59,** 1885–1897.

——, and M. W. Moncrieff, 1999: Effects of sea surface temperature and large-scale dynamics on the thermodynamic equilibrium state and convection over the tropical western Pacific. *J. Geophys. Res.,* **104,** 6093–6100.

——, W. D. Hall, W. W. Grabowski, M. W. Moncrieff, W. D. Collins, and J. T. Kiehl, 1999: Long-term behavior of cloud systems in TOGA COARE and their interactions with radiative and surface processes. Part II: Effects of ice microphysics on cloud–radiation interaction. *J. Atmos. Sci.,* **56,** 3177–3195.

Xu, K.-M., and D. A. Randall, 1999: A sensitivity study of radiative–convective equilibrium in the Tropics with a convection-resolving model. *J. Atmos. Sci.,* **56,** 3385–3399.

Yoshizaki, M., 1986: Numerical simulations of tropical squall-line clusters: Two-dimensional model. *J. Meteor. Soc. Japan,* **64,** 469–491.